

Commentary

On Modulating Interfacial Structure towards Improved Anti-Icing Performance

Kshitij C. Jha *, Emmanuel Anim-Danso, Selemon Bekele, George Eason † and Mesfin Tsige *

Received: 9 November 2015; Accepted: 6 January 2016; Published: 14 January 2016

Academic Editors: D. K. Sarkar and N. Saleema

Department of Polymer Science, The University of Akron, Akron, OH 44325, USA; ea25@zips.uakron.edu (E.A.-D.); selemon@uakron.edu (S.B.); gle7@zips.uakron.edu (G.E.)

* Correspondence: kcj4@uakron.edu (K.C.J.); mtsige@uakron.edu (M.T.); Tel.: +1-330-972-5631 (K.C.J. & M.T.)

† Current address: Department of Chemical Engineering, Christian Brothers University, Memphis, TN 38104, USA.

Abstract: The design of anti-icing surfaces presents an interface with high causal density that has been challenging to quantify in terms of individual contributions of various interactions and environmental factors. In this commentary, we highlight the role of interfacial water structure as uniquely expressing the physico-chemical aspects of ice accretion. Recent work on the topic that focuses on control of interfacial structure is discussed along with results by our research group on wettability of chemically modified surfaces and the role of ions in modulating interfacial structure. Suggestions for systematic studies to understand the fundamental interactions at play in ice adhesion at interfaces are made especially in the under-explored areas of cooperative hydrogen bonding and the role of solvated counterions. Insights expected from such studies would contribute to design of robust anti-icing hierarchies.

Keywords: anti-icing; interfacial structure; ice adhesion; ion segregation; superhydrophobicity; hierarchical design; biomimetic; chemically modified surfaces; quasi liquid layer; aqueous lubricating layer

1. Introduction

Understanding of ice nucleation mechanisms and their application to anti-icing solutions have been long-standing topics of scientific interest [1–18], with special focus on the area in the last decade [19–93]. As characterization methods and theoretical models have become more probative and computationally feasible, the surface science community has intensified efforts towards mitigating the major issue of icing on material surfaces. Innovative material design for improved anti-icing effectiveness has implications for improvement in safety and efficiency in a number of systems such as wind turbines, power transmission lines, and aircraft wings. As case examples, for wind turbines, ice accretion decreases the energy output while being a danger to people in the proximity of operation [94,95]; for power lines, approximately 3% are replaced each year due to degradation caused by heavy icing [96,97]; and for aircraft wings even thin layers of ice are a major safety hazard [98,99].

To counter the challenges of surface icing, active approaches have traditionally been deployed that remove accumulated ice through various mechanical and electrical methods. Surface treatment of substrates with de-icing fluids such as glycerol [100,101] (and recently ethylene glycol [102]) are also common. At the same time, the energy and time consumption and the need for periodic treatment make active solutions non-ideal and a “passive approach” through coatings or surface engineering that avoid conventional heating and salting are desired [103,104]. Increasing

interest in superhydrophobic [19,21,28,31,34,39,42,43,47,48,53,56,63,65,66,75,79–82,84,85,88–92,105–118], biomimetic [26,37,62,108,117,119–125], and textured [23,33,49,109,126–128] substrates and coatings, often with overlapping themes and principles, leads design in passive approaches to anti-icing. The major challenges for such designed surfaces in practical applications have been the adverse effects of droplet condensation (frosting) due to surface wear (post icing/de-icing cycles) [47,79]. It is commonly accepted that no universal solution to anti-icing exists, since the environments and modes of ice accretion vary widely [61]. Some of the approaches are laid out in Figure 1, with *self-lubricating layer* emphasized. Interfacial water structure (lubricating/quasi-liquid) and its effect on design of anti-icing surfaces is a focal point of this commentary.

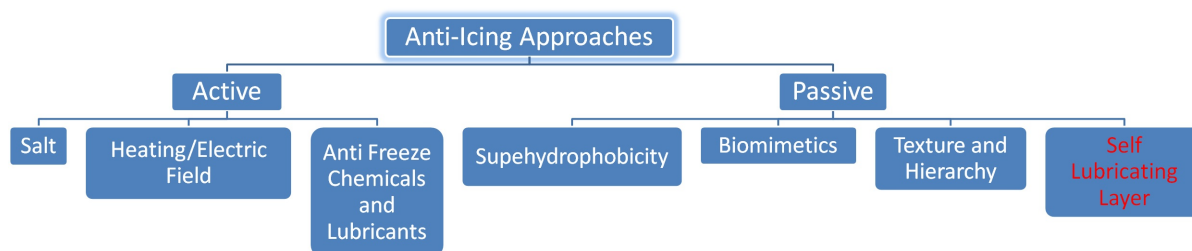


Figure 1. Schematic showing the major approaches towards anti-icing.

2. Factors Affecting Ice Accretion

2.1. Nucleation Mechanisms

The classical theory of Turnbull, Vonnegut, and Fletcher [129] has been used as a basis for examining heterogeneous ice nucleation on surfaces with varying wettability and phobicity [35,69] towards creating a thermodynamic framework that can lead to rational design of surfaces with freezing delays [130,131]. Figure 2A shows possible modes of freezing, homogeneous and heterogeneous, for an ideal water droplet. Environmental factors, such as evaporation, and presence of contaminants would play a role in homogeneous ice nucleation [6], direct computation of the rates of which have been attempted through coarse-grained models [87]. On flat, solid surfaces using a closed cell and accounting for the effects of evaporation and condensation, normalized rate of ice nucleation was found to be an order of magnitude higher for hydrophobic surfaces (Figure 2B).

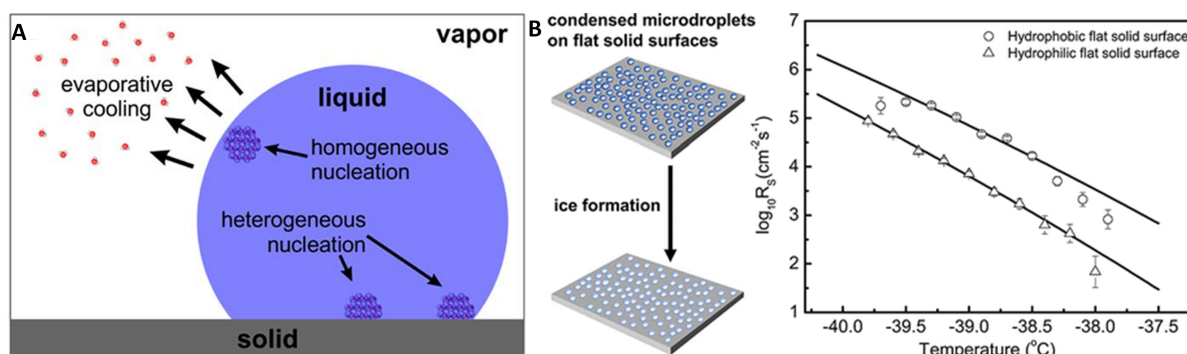


Figure 2. (A) Illustrates regions on a water droplet where homogeneous and heterogeneous ice nucleation occur and the influence of outside factors such as evaporation; (B) Shows the normalized surface ice nucleation rate for water microdroplets on flat, solid, hydrophobic and hydrophilic surfaces. Reprinted with permission from Refs. [32,130], respectively. ©2014 and ©2012 American Chemical Society.

2.2. Roughness and Wettability

From the observations above, it is apparent that one approach to decrease ice-adhesion would be to tune surface energy and roughness. Figure 3A is a computational analysis of the feasibility of this approach, using supercomputer based molecular dynamics (MD) simulations, wherein hydrophobicity is seen to suppress heterogeneous ice nucleation rates. However, if homogeneous nucleation occurs, and is self-propagating, then the effect of the surface would not be the determinant in preventing ice-adhesion. Figure 3B shows an increase in wettability with decrease in temperature, pointing to condensation being a limiting factor. The condensation of droplets, and the resultant frosting, leads to lack of robustness of superhydrophobic solutions to anti-icing. Robust anti-icing solutions are needed for both dynamic (aircraft wings) and static (power lines) applications [21].

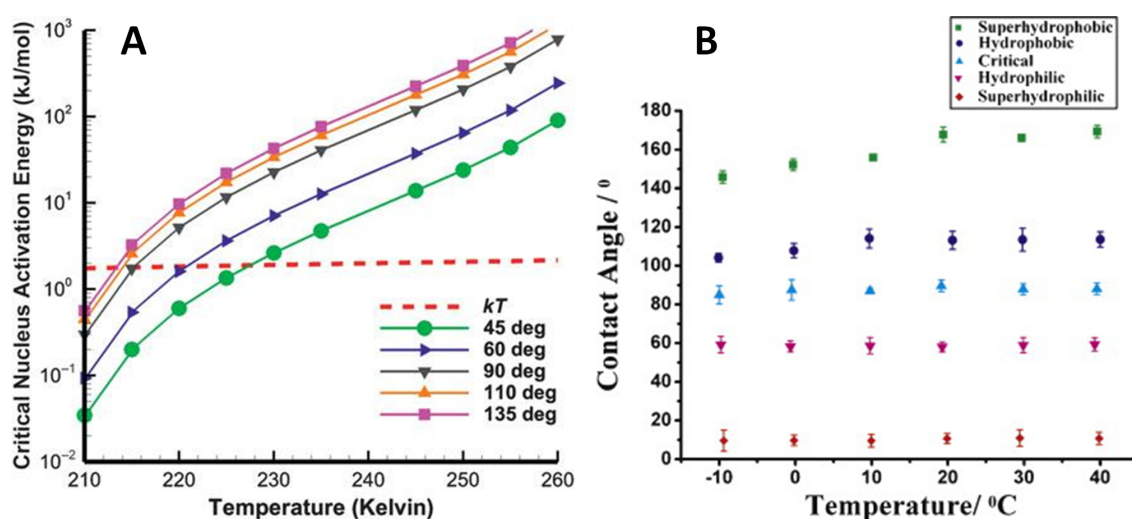


Figure 3. (A) Shows variation of activation energy for critical nucleation with temperature for different wettabilities. Red line represents region below which spontaneous freezing occurs; (B) Shows variation of contact angle with temperature for surface with differing wettabilities. Reprinted with permission from Refs. [22,61], respectively. ©2013 Materials Research Society; ©2010 Elsevier.

The effect of surface energy and roughness on adhesion has been studied by various groups [46,56,70,73,132,133], with varying conclusions. Campbell *et al.* [133] found experimentally insignificant dependence of nucleation of supercooled water droplets on surface roughness, for glass, silicon and mica surfaces. They attribute this effect to a liquid intermediate that aids vapor deposition. Fu *et al.* [46] carried a systematic study on sol-gel coatings with varying surface energies and roughness, shown in Figure 4A. As the amount of fluoroalkylsilane (FAS) weight% increases from 8% to 12%, there is a Wenzel to Cassie transition, which was shown in a large jump in measured contact angles from 110.3° for F-8 to 153.9° and 163.5° for F-12 and F-16, respectively. For formulations without FAS (M-x series, with silica nanoparticles), there is no such transition. The nucleation rates are two orders of magnitude higher for F-16, while all the M-x samples cluster together (Figure 4B,C). The authors hypothesize the nucleation behavior as occurring at the water-air-substrate contact line. Differences in test protocols, including size of droplets, surface microstructure, and environmental controls make it difficult to compare results from different research groups.

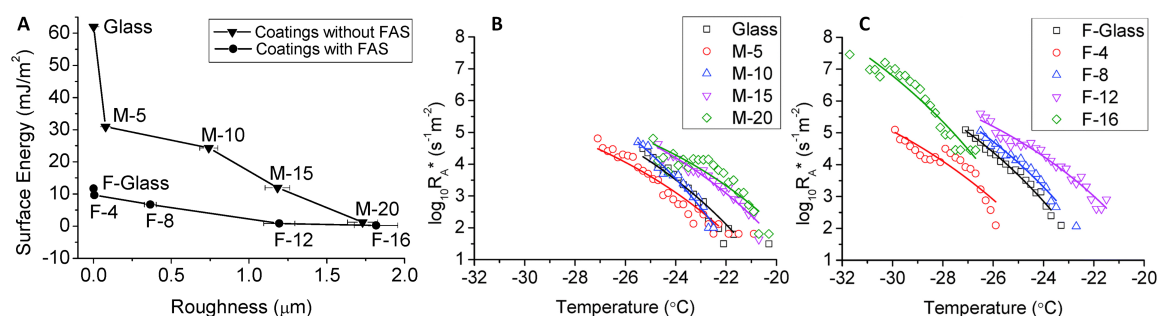


Figure 4. (A) Shows values for surface energy and roughness for two differing types of samples, with and without fluoroalkylsilane (FAS). Both samples are additionally loaded with silica nanoparticles. For M-x and F-x, x denotes the weight % of silica nanoparticles and FAS respectively; (B,C) Show variations in the area nucleation rate with temperature for the non-fluorinated and fluorinated samples. Reprinted with permission from Ref. [46]. ©2015 Royal Society of Chemistry.

2.3. Substrate Composition

Early work by Petrenko *et al.* [12,134] utilized change in surface chemical composition through use of self-assembled monolayers to decrease ice-adhesion. It can be seen in Figure 5 that increase in the degree of H-bonding would increase adhesion to the surface. Modulated hydrogen bonds, for control of interfacial structures that aid or impede ice nucleation, remains an under-explored area of design. It should be noted that the wettability, in large part, depends on near-surface chemical group density [111–114,135]. Understanding the fundamental interactions at chemically modified surfaces would allow design of interfaces critical to the development of the next generation of anti-icing solutions. It is to be noted that changes in near-surface concentration can occur not only through deposition of functional monolayers or surface oxidation of the substrate, but also through approaches that are more subtle, such as conformation of functional groups on the polymer backbone. For example, we have explored near-surface concentration as a function of stereoregularity (*viz.* tacticity) for a common polymer (PMMA) [136–138].

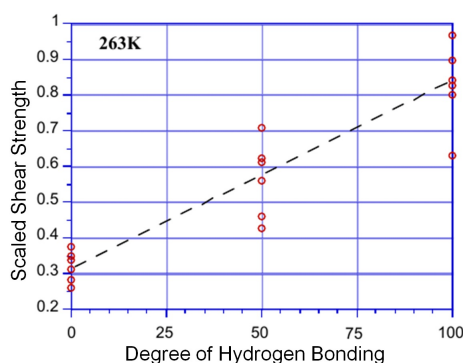


Figure 5. Scaled shear strength as a function of degree of hydrogen-bonding for different self assembled monolayers. Reprinted with permission from Ref. [134].

In cases where information on buried interfaces is needed for functional design, validated models would provide understanding of the role of various interactions in behaviors such as modulation of hydrogen bond networks and orientation profiles that would be challenging to obtain empirically. Our work on self-assembled monolayers [139] shows disruption of network by wetting that is in contrast to disruption through high temperature annealing (non symmetric response by wetting displayed in Figure 6). Examination of tilt angles, extending from surface bound sulphur to the end-terminal oxygens shows a zig-zag network for hydroxyl terminated n-alkanethiols.

The displayed H-bond contours from our simulation are very sensitive to external stimuli such as wetting and heating, exhibiting quantification of response unobtainable from spectroscopic methods. Since the strength of hydrogen-bond regulates the ice formation, or is at least a key contributor to it, examining the S–O tilt angle profiles for a number of supercooling rates would shed light on the correlation of ice nucleation with functional distribution of chemically modified surfaces (viz. percentage of hydroxylated species; density of end-terminal chemical groups).

Seminal work by Meuler *et al.* [25] showed that ice adhesion on chemically modified surfaces is almost linearly related to the practical work of adhesion, which is a function of the receding contact angle (Figure 7). Through modification brought by coating with fluorodecyl POSS, the limits on decrease in ice adhesion through chemical composition were reached, and it was argued that any further decreases would occur through changes in surface texture.

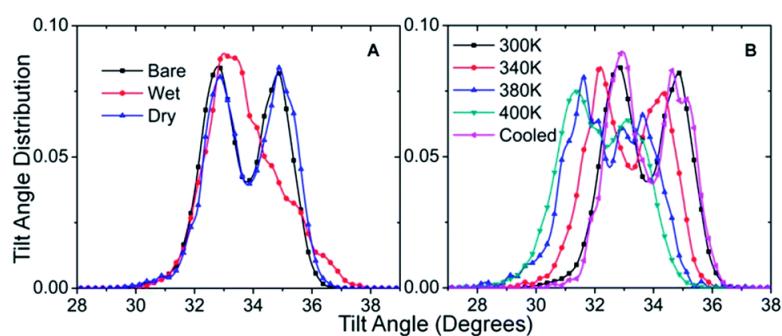


Figure 6. Effect of wetting and high temperature heating on hydrogen bond network of -OH terminated SAM. Reprinted with permission from Ref. [139]. ©2014 Royal Society of Chemistry.

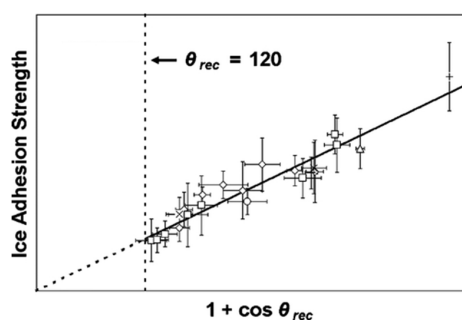


Figure 7. Ice adhesion strength as a function of practical work of adhesion. Reprinted with permission from Ref. [25]. ©2010 American Chemical Society.

2.4. Note on Ice Adhesion Measurements

The lack of common protocols and environmental standards for measuring ice-adhesion should serve as a note of caution to the reader when comparing results from different research groups [61]. Quantification of ice-adhesion includes measurements for shear, dynamic impact, and adhesion and wear strengths [140–144]. At the surface of a soft polymeric coat, the stress build depends on a number of factors, such as modulus strength of the polymer (K) and thickness of the coat (t) (Figure 8). A number of mechanisms, such as saltwater ice-adhesion [52,145] are not completely understood. Also, the adhesion strength changes markedly after icing/de-icing cycles, which will be discussed in the following section.

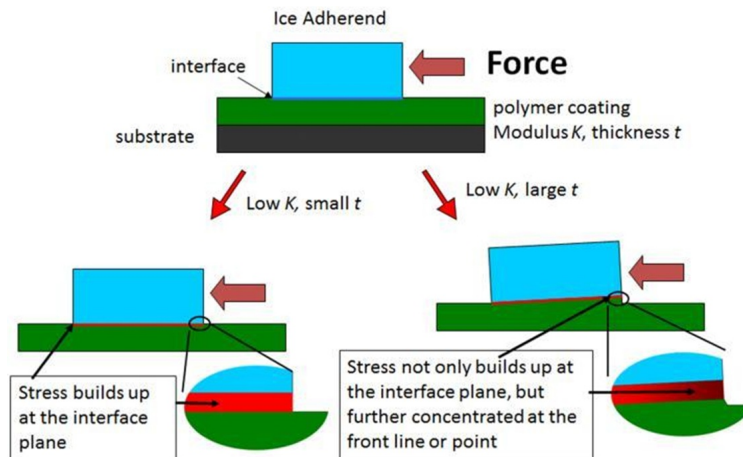


Figure 8. Effect of coating modulus (K) and thickness (t) on ice-removal through regulation of stress buildup at polymer soft coat interface. Reprinted with permission from Ref. [146]. ©2014 Virginia Commonwealth University.

3. Design Approaches to Anti-Icing

3.1. Wettability Models

Droplets on surfaces are traditionally described as being in the wettable Wenzel or the non-wettable Cassie-Baxter regime (Figure 9A). On superhydrophobic surfaces, by definition, droplets should be in the Cassie-Baxter state. Wearing down of the surface and infiltration through condensed water eventually would lead to Wenzel states. By careful design of asperities, slippery Wenzel states have recently been demonstrated [147]. The geometrical parameters allow for a critical angle of transition, wherein the Wenzel state is more favorable in designed nanotextured surfaces with additional incorporation of oils (Figure 9B).

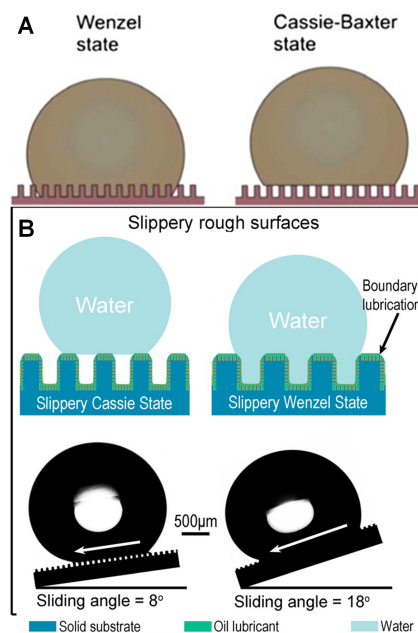


Figure 9. (A) Shows droplet in Wenzel (wetted) and Cassie-Baxter regimes (nonwetted); (B) Shows design of a hierarchical surface with slippery Wenzel regime through addition of oil lubricant to the pillars. Reprinted with permission from Refs. [79,147], respectively. ©2014 Elsevier; ©2015 American Chemical Society.

The competing factors in controlling wettability through phobicity are shown in Figure 10. Based on principles of accretion discussed in the preceding section, and the figure below, one innovative approach is to have a lubricating layer close to the substrate that would be enhanced by a hygroscopic component, while also allowing for a hydrophobic component that sheds water [29,40,41,55,148]. Antagonistic chemistry and hierarchical design principles are utilized for superhydrophobic, slippery liquid-infused porous substrates, and biomimetic approaches discussed in the subsections that follow.

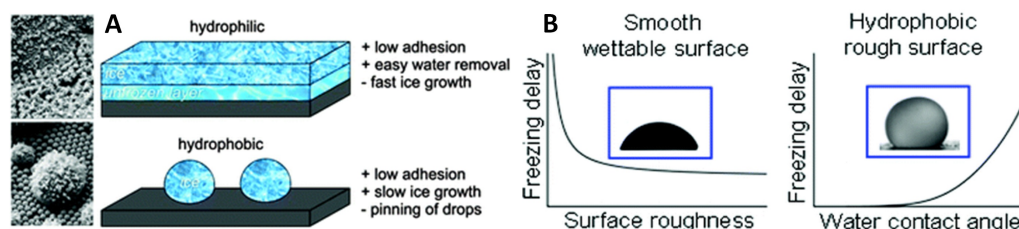


Figure 10. (A) Advantages and disadvantages of hydrophobic and hydrophilic surfaces in anti-icing design; (B) Competing effects of wettability and surface roughness in heterogeneous nucleation at hydrophobic surfaces. Reprinted with permission from Refs. [50,110], respectively. ©2015 Royal Society of Chemistry; ©2011 American Chemical Society.

3.2. Superhydrophobic Surfaces

Superhydrophobic surfaces show delayed nucleation which has been hypothesized as a consequence of lower heat transfer from the substrate [20,149]. Another contributing mechanism could be the decrease in water-substrate interfacial area, accompanied by an increase in free energy needed for nucleation [141]. Figure 11 shows changes of up to two orders of magnitude with differentials in interfacial area. The extreme effect of substrate temperature shown in Figure 11 is further exhibited in experimental measurements of droplet shedding for different wettabilities at a higher temperature range [150]. From these observations, one can infer that control in interfacial area of droplet-substrate through surface modification is a relevant factor in the technological design of anti-icing surfaces.

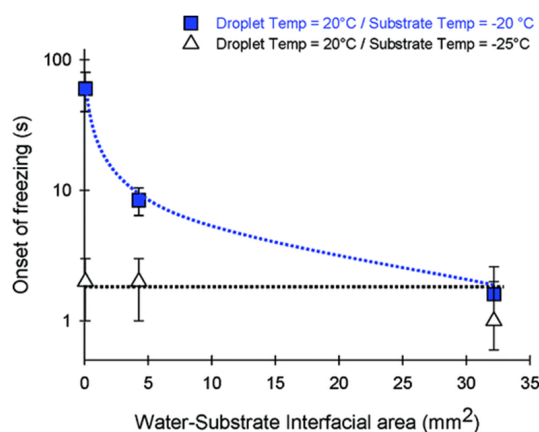


Figure 11. Freezing onset as a function of the interfacial area of contact between the substrate and the droplet for two different substrate temperatures. Reprinted with permission from Ref. [141]. ©2012 American Chemical Society.

The robustness of superhydrophobic surfaces has raised questions per their icephobic efficacy [21,47,110]. Kulinich *et al.* [132] show a clear increase in ice-adhesion for three different samples with contact angles near or in excess of 150° with increase in number of (icing/de-icing)

cycles (Figure 12). Wear of coatings and surfaces leads to transition from an ideal Cassie to a non-desirable Wenzel regime and corresponding increase in surface contact area. In a study comparing all the factors that contribute to an ideal robust icephobic surface, Schutzius *et al.* posit that a micro-/nano-scale multi-tier texture has the best resistance to droplet impalement as well as ice nucleation [130].

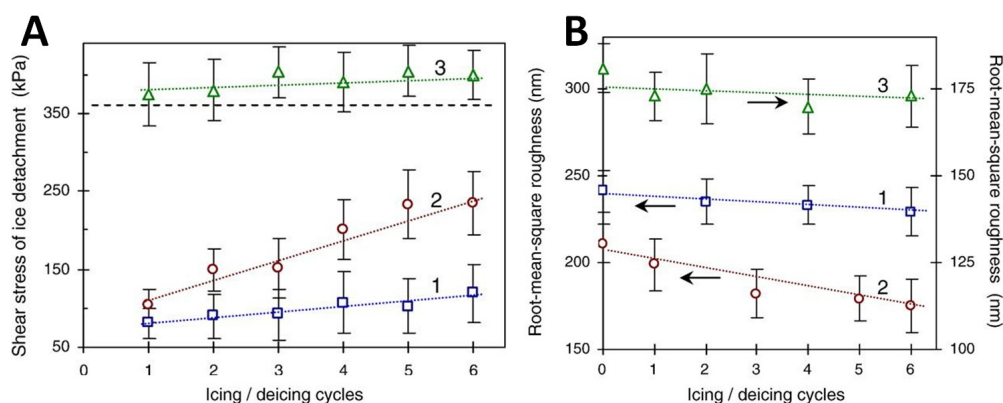


Figure 12. The effect of icing/de-icing cycles on (A) ice adhesion and (B) surface roughness, measured for “artificial” glaze ice for three samples with high contact angles (>150°). Reprinted with permission from Ref. [132]. ©2011 Elsevier.

3.3. Slippery Liquid Infused Porous Surfaces (SLIPS)

In concurrence with the design principle that maintaining a lubricating layer prevents ice adhesion, SLIPS were designed by the Aizenberg group with remarkable roll off properties [30,36]. However, as Figure 13 illustrates, non-functional SLIPS after wear may have the additional issue of oil depletion upon frost formation.

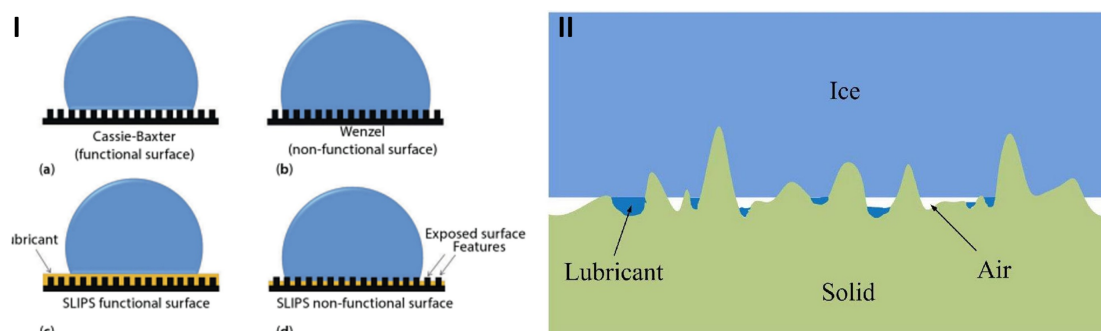


Figure 13. (I) Schematic for (a) Cassie-Baxter; (b) Wenzel; (c) functional Slippery Liquid Infused Porous Surfaces (SLIPS); and (d) non-functional SLIPS interfaces; (II) Illustration of a realistic contact pattern between ice and substrate for lubricant infused interfaces. Reprinted with permission from Refs. [151,152], respectively. ©2015 John Wiley & Sons; ©2015 Elsevier.

3.4. Biomimetic Design

Hierarchical approach to biomimetic design has grown beyond the initial lotus-leaf inspiration, to creatures such as tropical frogs that secrete toxins when provoked. Building on a stimuli based approach, the Rykaczewski group [62] formed a bilayer structure with antifreeze reservoir bottom and a superhydrophobic porous top (Figure 14), which leaches the antifreeze on frost formation.

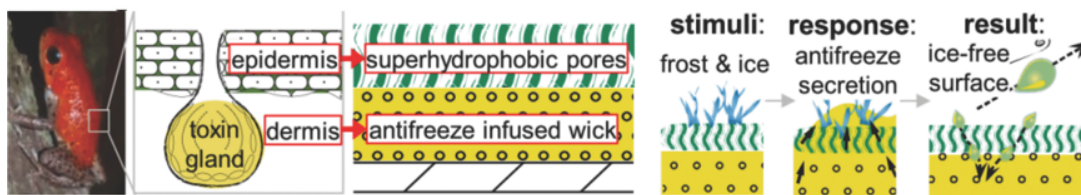


Figure 14. A two-layered coating, inspired by frog’s skin that secretes anti-freeze as a response to ice accretion. Reprinted with permission from Ref. [62]. ©2015 Wiley Online Library.

A less complex hierarchy of superhydrophilic polyelectrolyte brushes hosting ions is also along the lines of inspiration from natural processes such as cloud and hydrate formation. The “hosted ion” architecture, an under-explored design theme, is able to control ice adhesion through a dispersed ion population with varying results for different ions [153,154]. For a Li^+ ion, the reduction (in ice adhesion) is *ca.* 70% at $-10\text{ }^\circ\text{C}$, while for Ag^+ ion the corresponding reduction is by 80%. It is hypothesized that highly hydrated ions form a quasi-liquid layer (QLL) that impedes ice nucleation. The coordination of ions is directly related to the formation of QLL, with the temperature-thickness dependence a stated empirical challenge [155–158] that would be aided by a molecular understanding of the QLL structure. A larger hydration shell would correspond to increased order or negative entropy. Using “water structural entropy” as a quantifier of degree of hydration, ΔS_{struct} was found to be $-52\text{ J K}^{-1}\text{ mol}^{-1}$ for Li^+ , and $+47\text{ J K}^{-1}\text{ mol}^{-1}$ for K^+ [159], which correlates well with decreased ice-adhesion for Li^+ and no effect on ice-adhesion for K^+ ions in the brushes, especially at $-18\text{ }^\circ\text{C}$ (Figure 15). While ion coordination affects ice formation, their dissociation is also key to improved anti-icing effect. The dissociation effect can be observed in Figure 15 wherein circles represent higher dissociation for sulfonate groups, and triangles represent lower dissociation for carboxylate groups as part of the brushes with different cations. Further, multivalent ions, even when exhibiting high hydration, change the overall structure of the polyelectrolyte brushes leading to negative effects in anti-icing efficacy. Figure 15 summarizes the ice-adhesion properties for a range of host-guest ion incorporated brushes, and shows the effects of competing factors at play [153].

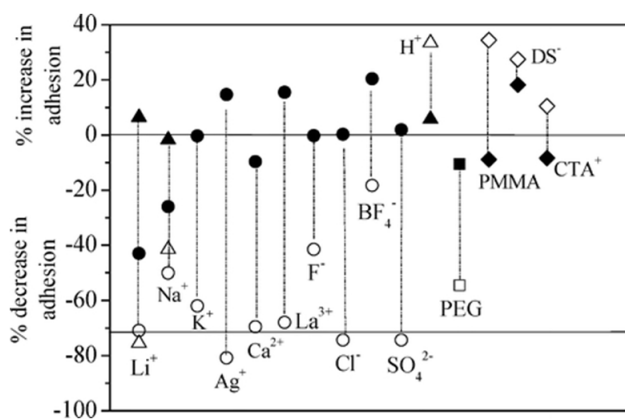


Figure 15. Changes in ice-adhesion for different ions incorporated in polyelectrolyte brushes. Filled symbols represent measurements at $-18\text{ }^\circ\text{C}$, while open symbols represent measurements at $-10\text{ }^\circ\text{C}$. Reprinted with permission from Ref. [153]. ©2014 American Chemical Society.

4. Role of Interfacial Water

Near-surface concentration is key to the control of phobicity and can be expressed in terms of the structure of interfacial water. We observe in Figure 16A that increase in silanol concentration leads to variance in packing, and increase in ice-like behavior of water. Water structuring, measured through viscosity under confinement, shows increase at different separations (3–8 nm) for different

silanol densities [160]. For polymeric surfaces, we examined the effect of surface oxidation and found almost a linear dependence of degree of wettability on surface oxidation for atactic Polystyrene (Figure 16B) [161]. This is important for many applications in biocompatibility, where the same principles of solvation shells in interfacial water structure, and displacement of proteins with water result in tunable biomacromolecular adhesion [162–164]. There are distinct design implications of changes in near-surface concentration for amphiphilic anti-icing hierarchies [153] discussed earlier, as also the design and performance of de-icing macromolecules. For example, the surface conformations of ethylene glycol (EG) and its behavior as a hydrogen-bond acceptor which leads to various solvation shells at the EG-water interface and low probability of EG-EG complexation has been noted as key to its anti-icing behavior [102]. Such an approach through tunable hydrogen bond coupling allows for programmable surfaces [165], and design of mimetic antifreeze materials based on traditionally employed structures such as PVA [166].

While the role of hydrogen bond in modulating interfacial behavior is to be expected, hydrogen bond interactions are one of the many factors that contribute to final accretion. The relative roles of roughness, supercooling rate, and other non-bond interactions such as van der Waals forces needs quantification for guided design of coatings and hierarchical substrates. Wetting under confinement with varying levels of phobicity would provide such information, and has been the focus of recent studies by our collaborators [167,168].

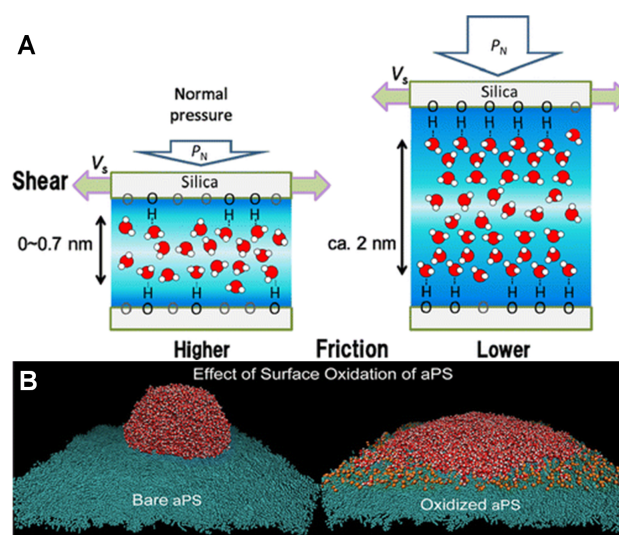


Figure 16. Changes in interfacial water behavior for varying levels of surface oxygen enrichment. (A) Shows resonance shear measurements for plasma treated and untreated silica surfaces with differing silanol densities; (B) Shows spreading of water on untreated and oxidized atactic Polystyrene. Reprinted with permission from Refs. [160,161], respectively. ©2013 American Chemical Society.

4.1. Quasi Liquid Layer (QLL)

A striking role that interfacial water structure plays is in the formation, geometry and thickness of the quasi-liquid layer [169], the thickness and nature of which is much debated. In Figure 17A we can see the pre-melt layer wetting the interface between substrate and ice. This could serve as a self lubricating layer, if it can be regulated. The ice accretion is often modeled as supercooled water droplets on the substrate [44]. At the same time, the nature of the wetting layer would govern, and could be correlated to the ice-adhesion. Disruption of the QLL through charge, pH, and local electric fields would also be possible. This would have an impact on the heterogeneous ice nucleation mechanism for confinement in curvatures shown in Figure 17A.

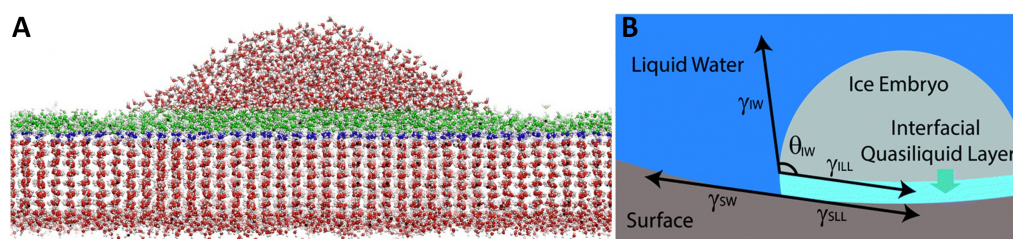


Figure 17. (A) Pre-melting quasi-liquid layer (QLL) at the ice-water interface; (B) Heterogeneous nucleation in a nanopit that shows ice embryo and interfacial quasi-liquid layer (QLL). Reprinted with permission from Refs. [131,169], respectively. ©2014 Elsevier; ©2014 Royal Society of Chemistry.

Along these same principles, designed interaction through formation of hydrogen bonds pre- and post-perturbation leads to a self-healing process that can be used for anti-fogging applications (Figure 18C). We also observe that the water structure close to an intrinsically hydrophobic surface such as rare earth metal oxide is much different than alumina (Figure 18A,B). Similar to these design approaches, control of QLL, wherein the water structure, its orientation and hydrogen bond formation can be modified, presents an opportunity for hierarchical design and delayed ice nucleation.

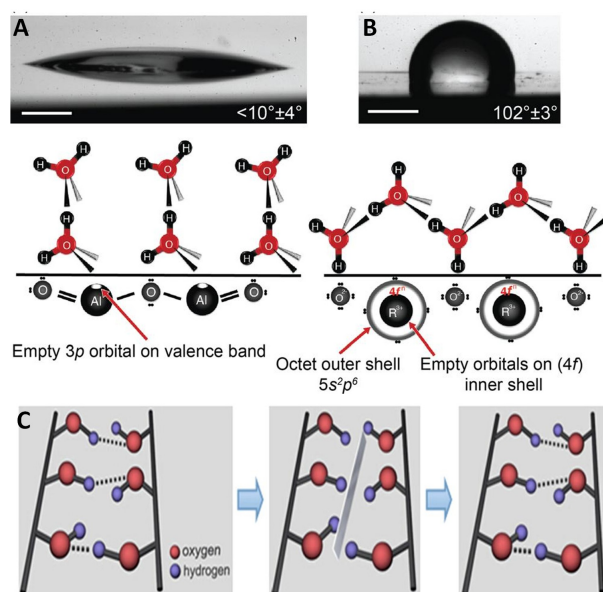


Figure 18. (A) and (B) Represent wettability and water molecule orientation for an alumina and a neodymia (Rare Earth Oxide) surface, respectively; (C) Illustrates the hydrogen-bond modulated self-healing for a polymer thin film designed for anti-fogging applications. Reprinted with permission from Refs. [170,171], respectively. ©2015 AIP Publishing; ©2015 Nature Publishing Group.

4.2. Role of Ions at the Interface

The complex behavior of ions has long been a puzzle for colloidal and protein based behavior at interfaces (Figure 19A) ever since the Hofmeister series was first proposed [172], and the various physico-chemical aspects are still not completely understood [173,174]. While anions have the stronger impact in the behaviors listed in Figure 19A, counter-ion solvation also leads to differentials in biomacromolecular adsorption (Figure 19B) which can be expressed in terms of adsorption energies, conformational changes, and adhesive properties [175–179]. The effect on coagulation of polystyrene latex particles for both anions and cations [180] is shown in Figure 19C.

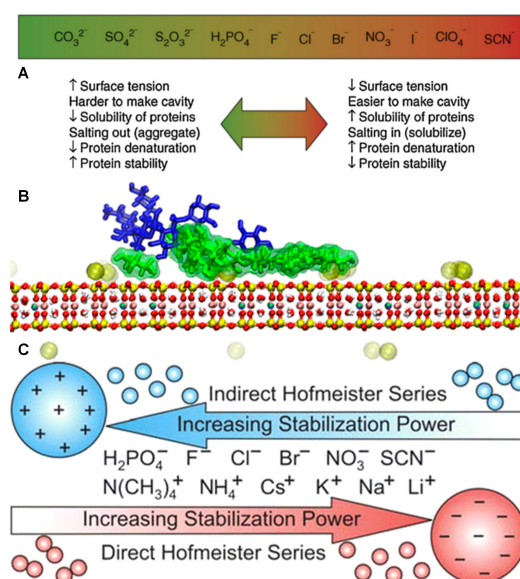


Figure 19. Effect of cations and anions at the interface. (A) Shows Hofmeister effect for anions and their physico-chemical implication; (B) Shows effect of counterion hydration on adhesion at a clay surface; (C) Shows effect of cations and anions on stabilization of polystyrene latex particles. Reprinted with permission from Refs. [174,175,180], respectively. ©2006 Elsevier; ©2014 American Chemical Society; ©2015 American Chemical Society.

Control of type and distribution of ions is a parameter that could be additionally exploited to disrupt the interfacial water structures as shown for the case of polyelectrolyte brushes (Figure 15). Additionally, the degree of substrate surface charge would control concentration and distribution of ions close to interfaces where ice accretion would occur, and hence influence the interfacial water structure. Traditionally, the role of ions in ice nucleation has been studied in atmospheric and geochemical contexts [181–183] and there is ambiguity in the exact mechanisms of ion-mediated ice nucleation [184–187]. Close to the interface, depending on local fields, the oxygens can point up or down (measured as a vector from hydrogen to oxygen), leading to variations in local structure and differentials in coordination geometry of ice formations (hexagonal *vs.* tetrahedral) [87,103,188]. The hydrogen bonds towards the bulk are termed as “bilayer stitching” bonds, and have been hypothesized as the major contributor to the intense H-bonded band in sum frequency generation (SFG) spectra of ice [189,190]. Charge transfer in the stitching bilayer could control local ordering [184], and a systematic study of the orientation profiles of interfacial water and ions would provide insight into the mechanisms at play for ice nucleation near solid surfaces. For a negatively charged surface, a proton disordered ice structure was observed compared to a proton ordered structure for positively charged surface [184].

4.3. Sum Frequency Generation and Molecular Dynamics Results

A systematic analysis of the freezing of water next to sapphire surfaces through sum frequency generation (SFG) spectroscopy was done by our collaborators [184]. Sapphire was chosen because of the wide range of interaction strengths [191] possible through tunable hydroxylation (*viz.* change in pH) as evidenced by room temperature contact angle measurements [192]. The spectra for pH 9.8 showed significantly lowered intensities compared to pH 3.3 near the transition temperatures (Figure 20), while the melting and freezing transition temperatures themselves did not change. A two-step transition is seen at pH 9.8 and it has been hypothesized that the disruption of the stitching bilayer and charge transfer through the presence of Na^+ ions contributes to both reduction in signal intensity and differences in the nature of transition.

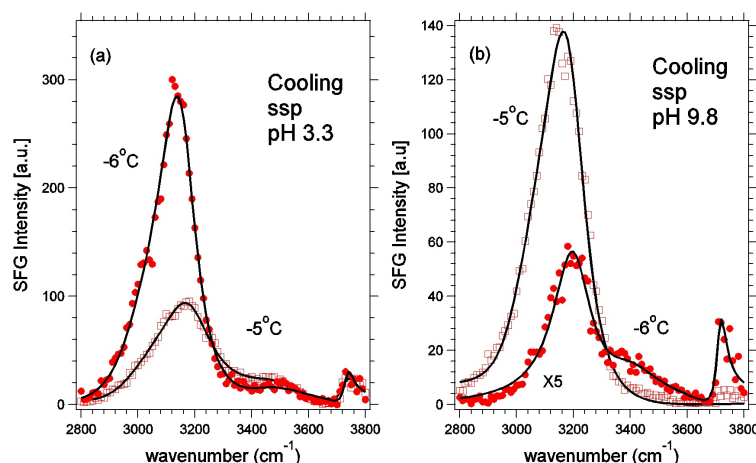


Figure 20. Sum frequency generation (SFG) collected in SSP polarization during cooling for two different pH scales. Water is represented as open squares while ice is shown by filled circles with the spectra showing transitions near the freezing and melt temperatures. Reprinted with permission from Ref. [184]. ©2013 American Chemical Society.

To analyze changes in behavior of water at sapphire surfaces with surface charge, we performed all-atom molecular dynamics (MD) simulations for neutral and 20% negatively charged surfaces. An α -sapphire surface of approximately 26 Å in thickness was used representing a complete replication of the hexagonal lattice along the c-axis through 6 O^{2-} and 6 intermediate Al^{3+} layers. The unit cell was replicated along the a and b dimensions for an area of approximately $54 \times 50 \text{ Å}^2$ in the XY plane. 20% negative charge was imparted through random removal of hydrogens from the ($-OH$ terminated) sapphire surface. Water films of 30 and 100 Å thickness were placed on top of the sapphire surface corresponding to 2276 and 7779 water molecules, respectively. All simulations were run for 2.5 ns with an integration timestep of 0.5 fs. The sapphire surface was treated using the CLAYFF force field [193] while the water molecules were treated using a SPC/E model [194,195].

We observed significant changes in ordering and layering close to the 20% negatively charged α -sapphire surface. The θ values in Figure 21 represent the dipole angles of water molecules with respect to the normal to the surface. The probability distribution for θ shown in Figure 21A reveals peaks for the first and second layer that are close to 130° indicating that the hydrogens are facing towards the α -sapphire surface. Interestingly, the second layer has a sharper peak than the first, which may be caused by a templating effect of the first layer. This has been reported in recent MD simulations of ice growth on facets of varying roughness [69] with a water overlayer acting as an in-plane template. The distribution shows equal probability, as expected, for the case of bulk water.

We next compare the time averaged $\cos(\theta)$ values for charged *versus* neutral surfaces, shown in Figure 21B. The layers of water close to the charged surface are significantly more ordered when compared to the neutral surface as shown by the sharp dip between 0–10 Å. The neutral surface quickly recovers to random distribution (displaying bulk behavior) around 10 Å and the ordering of the water surface close to the neutral sapphire surface (below 10 Å) is not as pronounced as for the charged sapphire surface (Figure 21C). It should be noted that the peak at the end in the opposite direction is at the water-air interface, where the density of water molecules indicates the presence of vapor phase. The hydrogens for a water molecule point towards the air, at the air-water interface, and towards sapphire, at the sapphire-water interface. On the charged surface, since we have not achieved bulk behavior even in the 100 Å water film, ordering anywhere in the film would be a combined contribution of water-air interface and water-sapphire interface. The layering shown by the density distribution also points to the charged surface having the first two layers at density almost twice that of pure bulk water. Such layering is more significant for the charged surface by approximately 30% when compared to the neutral surface (not shown).

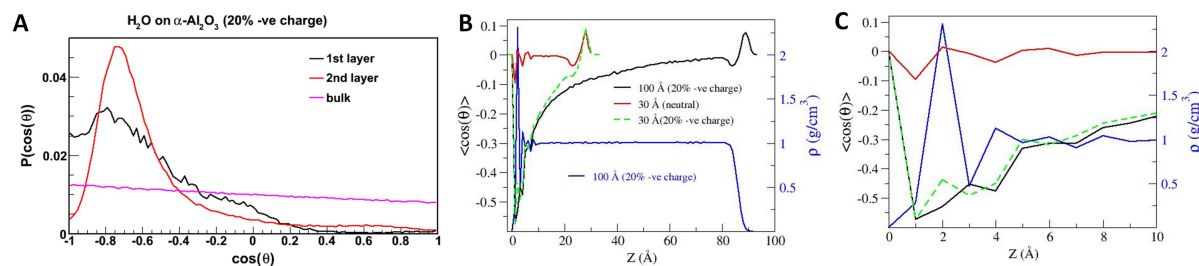


Figure 21. Effect of surface charge and thickness of water layer on the structuring of interfacial water at charged and neutral sapphire surfaces. (A) Shows the probability of the cosine of the dipole angle (θ) of water, measured with respect to the surface normal, for the first, and second water layers at a charged sapphire surface as well as for bulk water for comparison; (B) Shows time averaged $\cos(\theta)$ values for two different thicknesses of water at charged sapphire surface and a comparison with neutral sapphire surface. Also shown is the density distribution for 100 Å thickness of water on the charged sapphire surface; (C) Shows the zoomed in picture for the first 10 Å.

Since the ordering due to the negatively charged surface travels through the entirety of the 30 Å water film, we analyzed the effect of placing a larger film of water. As can be observed in Figure 21B, ordering of the water structure close to the negatively charged sapphire surface overlaps for the first few layers for both 30 and 100 Å films. Further, the effect of this ordering travels through the 100 Å film, with a gentler gradient after approximately 18 Å. This deviation is a result of the additive effect of ordering at the two water interfaces (air and sapphire) being different for the two thicknesses. For water on the charged sapphire surface even for a large thickness (100 Å of water), the ordering does not become random as observed for the neutral sapphire surface. This implies that ordering of the water structure on negatively charge surfaces is large, and may require an even thicker water layer for it to become random and show bulk behavior. The results from all-atom MD are in accordance with the hypothesis from SFG spectra that points to higher changes in ordering for a charged surface, in comparison to a neutral surface, when traveling away from the water-sapphire interface.

5. Conclusions and Outlook

With an overview of the mechanisms, factors, and design principles utilized in the current anti-icing hierarchies, we propose that robust design can additionally benefit from an analysis of the interfacial water structure. The design principles tell us that a self lubricating layer delays ice adhesion and is to be preferred in considering anti-icing solutions. The nature of quasi-liquid layer (QLL) and the role of ions close to the surface are not understood in terms of their effect on ice adhesion or nucleation. Mimetic designs based on hydrophilic brushes have attempted to utilize the anomalous hydration and entropic behavior of ions.

“Shape disrupting” *versus* “shape forming” ions, with different values for water structural entropy, delay ice adhesion by varying degrees. The thickness dependence of QLL on hydration shells and temperature and its correlation to nucleation remains an open question. While the role of cations has been traditionally examined in geological, atmospheric, bio-adhesion, and hydrate formation contexts, its effect on heterogeneous ice nucleation for anti-icing surface design needs further study.

Our outlook on the topic is that there exists a need for understanding of the interfacial water structure and its behavior with changes in ion distribution and local environments common to material applications being sought. Based on this understanding, a hierarchical design of interfaces can be proposed that selectively disrupts and delays nucleation in a given set of environments. We show initial MD results, in good agreement with the overall mechanistic understanding from SFG, that can be further developed for rational design of environmentally responsive ice-phobic materials, mimics, and coats.

Acknowledgments: This work was made possible by funding from the ACS Petroleum Research Fund (ACS PRF 54801-ND5). G.E. acknowledges financial support through the NSF REU program in the College of Polymer Science and Polymer Engineering at The University of Akron (NSF REU DMR-1359321). E.A.-D. acknowledges work performed in the laboratory of Ali Dhinojwala.

Author Contributions: M.T. conceived and designed the project. All authors contributed to analysis of results and writing of the commentary.

Conflicts of Interest: The authors declare no conflict of interest.

References

1. Harry, L.W.; Alexander, R.O. Compositions for the Prevention of the Formation or Accretion of Ice on Exposed Surfaces. U.S. Patent 2,373,727, 1945.
2. Sayward, J.M. *Seeking Low Ice Adhesion*; Special report (Cold Regions Research and Engineering Laboratory (U.S.); The Laboratory: Hanover, NH, USA, 1979).
3. Nimerick, K.H.; Copeland, C.T. Composition and Method for Melting Frozen Aqueous Solutions. U.S. Patent 4,388,203, 1983.
4. Rosen, K.; Potash, M. Forty years of helicopter ice protection experience at sikorsky aircraft. *J. Am. Helicopter Soc.* **1981**, *26*, 5–19.
5. Kanury, A.; McComas, S.; Lloyd, J.; Slepicka, K.; Miller, A.; Kosel, T.; Strieder, W.; Wolf, E. *Cold Weather Transit Technology Program. Volume 2: Physics of Ice and Snow at the Interface with Transitway Surfaces*; Technical Report; U.S. Department of Transportation, Urban Mass Transportation Administration: Washington, DC, USA, 1981.
6. Pruppacher, H. A new look at homogeneous ice nucleation in supercooled water drops. *J. Atmos. Sci.* **1995**, *52*, 1924–1933.
7. Hansman, R.J., Jr.; Dershowitz, A. Optically Indicating Surface De-Icing Fluids. U.S. Patent 5,039,439, 1991.
8. Gent, R.; Dart, N.; Cansdale, J. Aircraft icing. *Philos. Trans. R. Soc. Lond. A Math. Phys. Eng. Sci.* **2000**, *358*, 2873–2911.
9. Worsnop, D.R.; Miake-Lye, R.; Hed, Z.E. *Icing Prevention by Ultrasonic Nucleation of Supercooled Water Droplets in Front of Subsonic Aircraft*; U.S. Department of Transportation: Washington, DC, USA, 1992.
10. Cheng, K.; Yen, Y.C. Historical and Recent Developments in the Research of Cold Regions Heat Transfer—Ice in Air, Water, and Earth. In *Freezing and Melting Heat Transfer in Engineering: Selected Topics on Ice-Water Systems and Welding and Casting Processes*; CRC Press: Boca Raton, FL, USA, 1991; p. 17.
11. Rasmussen, R.M.; Crook, A.; Kessinger, C. Snow-band formation and evolution during the 15 November 1987 aircraft accident at Denver airport. *Weather Forecast.* **1993**, *8*, 453–480.
12. Petrenko, V.; Peng, S. Reduction of ice adhesion to metal by using self-assembling monolayers (SAMs). *Can. J. Phys.* **2003**, *81*, 387–393.
13. Wowk, B. Polyvinyl Alcohol Compounds for Inhibition of Ice Growth. U.S. Patent 6,391,224, 2002.
14. Cober, S.G.; Isaac, G.A. Aircraft icing environments observed in mixed-phase clouds. In Proceedings of the AIAA 40th Aerospace Sciences Meeting & Exhibit, Reno, NV, USA, 14–17 January 2002.
15. Myers, T.; Charpin, J.; Thompson, C. Slowly accreting ice due to supercooled water impacting on a cold surface. *Phys. Fluids (1994-Present)* **2002**, *14*, 240–256.
16. Cortinas, J.V., Jr.; Bernstein, B.C.; Robbins, C.C.; Strapp, J.W. An analysis of freezing rain, freezing drizzle, and ice pellets across the United States and Canada: 1976–90. *Weather Forecast.* **2004**, *19*, 377–390.
17. Georgiadis, J.G.; Hoke, J. Quantitative Visualization of Early Frost Growth with Scanning Confocal Microscopy. In Proceedings of the Brazilian Congress of Thermal Engineering & Science, Rio de Janeiro, Brazil, 30 November–4 December 2004.
18. Hanson, B.L.; Schall, C.A.; Bunick, G.J. New techniques in macromolecular cryocrystallography: Macromolecular crystal annealing and cryogenic helium. *J. Struct. Biol.* **2003**, *142*, 77–87.
19. Cao, L.; Jones, A.K.; Sikka, V.K.; Wu, J.; Gao, D. Anti-icing superhydrophobic coatings. *Langmuir* **2009**, *25*, 12444–12448.
20. Mishchenko, L.; Hatton, B.; Bahadur, V.; Taylor, J.A.; Krupenkin, T.; Aizenberg, J. Design of ice-free nanostructured surfaces based on repulsion of impacting water droplets. *ACS Nano* **2010**, *4*, 7699–7707.

21. Varanasi, K.K.; Deng, T.; Smith, J.D.; Hsu, M.; Bhate, N. Frost formation and ice adhesion on superhydrophobic surfaces. *Appl. Phys. Lett.* **2010**, *97*, 234102.
22. Yin, L.; Xia, Q.; Xue, J.; Yang, S.; Wang, Q.; Chen, Q. *In situ* investigation of ice formation on surfaces with representative wettability. *Appl. Surf. Sci.* **2010**, *256*, 6764–6769.
23. Meuler, A.J.; McKinley, G.H.; Cohen, R.E. Exploiting topographical texture to impart icephobicity. *ACS Nano* **2010**, *4*, 7048–7052.
24. Ayres, J.; Simendinger, W.; Balik, C. Characterization of titanium alkoxide sol–gel systems designed for anti-icing coatings: II. Mass loss kinetics. *J. Coat. Technol. Res.* **2007**, *4*, 473–481.
25. Meuler, A.J.; Smith, J.D.; Varanasi, K.K.; Mabry, J.M.; McKinley, G.H.; Cohen, R.E. Relationships between water wettability and ice adhesion. *ACS Appl. Mater. Interfaces* **2010**, *2*, 3100–3110.
26. Grunwald, I.; Rischka, K.; Kast, S.M.; Scheibel, T.; Bargel, H. Mimicking biopolymers on a molecular scale: Nano (bio) technology based on engineered proteins. *Philos. Trans. R. Soc. Lond. A Math. Phys. Eng. Sci.* **2009**, *367*, 1727–1747.
27. Alizadeh, A.; Bahadur, V.; Zhong, S.; Shang, W.; Li, R.; Ruud, J.; Yamada, M.; Ge, L.; Dhinojwala, A.; Sohal, M. Temperature dependent droplet impact dynamics on flat and textured surfaces. *Appl. Phys. Lett.* **2012**, *100*, 111601.
28. Shen, Y.; Tao, J.; Tao, H.; Chen, S.; Pan, L.; Wang, T. Anti-icing potential of superhydrophobic Ti6Al4V surfaces: Ice nucleation and growth. *Langmuir* **2015**, *31*, 10799–10806.
29. Chen, J.; Dou, R.; Cui, D.; Zhang, Q.; Zhang, Y.; Xu, F.; Zhou, X.; Wang, J.; Song, Y.; Jiang, L. Robust prototypical anti-icing coatings with a self-lubricating liquid water layer between ice and substrate. *ACS Appl. Mater. Interfaces* **2013**, *5*, 4026–4030.
30. Kim, P.; Wong, T.S.; Alvarenga, J.; Kreder, M.J.; Adorno-Martinez, W.E.; Aizenberg, J. Liquid-infused nanostructured surfaces with extreme anti-ice and anti-frost performance. *ACS Nano* **2012**, *6*, 6569–6577.
31. Wang, Y.; Xue, J.; Wang, Q.; Chen, Q.; Ding, J. Verification of icephobic/anti-icing properties of a superhydrophobic surface. *ACS Appl. Mater. Interfaces* **2013**, *5*, 3370–3381.
32. Li, K.; Xu, S.; Shi, W.; He, M.; Li, H.; Li, S.; Zhou, X.; Wang, J.; Song, Y. Investigating the effects of solid surfaces on ice nucleation. *Langmuir* **2012**, *28*, 10749–10754.
33. Charpentier, T.V.; Neville, A.; Millner, P.; Hewson, R.W.; Morina, A. Development of anti-icing materials by chemical tailoring of hydrophobic textured metallic surfaces. *J. Colloid Interface Sci.* **2013**, *394*, 539–544.
34. Ruan, M.; Li, W.; Wang, B.; Deng, B.; Ma, F.; Yu, Z. Preparation and anti-icing behavior of superhydrophobic surfaces on aluminum alloy substrates. *Langmuir* **2013**, *29*, 8482–8491.
35. Charpentier, T.V. The Heterogeneous Ice Nucleation Properties of Structured and Chemically Tailored Surfaces for the Development of Novel Anti-Icing Materials. Ph.D. Thesis, University of Leeds, Leeds, UK, 2012.
36. Wilson, P.W.; Lu, W.; Xu, H.; Kim, P.; Kreder, M.J.; Alvarenga, J.; Aizenberg, J. Inhibition of ice nucleation by slippery liquid-infused porous surfaces (SLIPS). *Phys. Chem. Chem. Phys.* **2013**, *15*, 581–585.
37. Lv, J.; Song, Y.; Jiang, L.; Wang, J. Bio-inspired strategies for anti-icing. *ACS Nano* **2014**, *8*, 3152–3169.
38. Arianpour, F.; Farzaneh, M.; Kulinich, S. Hydrophobic and ice-retarding properties of doped silicone rubber coatings. *Appl. Surface Sci.* **2013**, *265*, 546–552.
39. Zhan, X.; Yan, Y.; Zhang, Q.; Chen, F. A novel superhydrophobic hybrid nanocomposite material prepared by surface-initiated AGET ATRP and its anti-icing properties. *J. Mater. Chem. A* **2014**, *2*, 9390–9399.
40. Dou, R.; Chen, J.; Zhang, Y.; Wang, X.; Cui, D.; Song, Y.; Jiang, L.; Wang, J. Anti-icing Coating with an Aqueous Lubricating Layer. *ACS Appl. Mater. Interfaces* **2014**, *6*, 6998–7003.
41. Nowak, A.P.; Gross, A.F.; Bartl, M.H. Structural Coatings with Dewetting and Anti-Icing Properties, and Coating Precursors for Fabricating Same. U.S. Pat. App. 13/708,642, 2012.
42. Fang, G.; Amirfazli, A. Understanding the anti-icing behavior of superhydrophobic surfaces. *Surface Innov.* **2014**, *2*, 94–102.
43. Jung, M.; Kim, T.; Kim, H.; Shin, R.; Lee, J.; Lee, J.; Lee, J.; Kang, S. Design and fabrication of a large-area superhydrophobic metal surface with anti-icing properties engineered using a top-down approach. *Appl. Surf. Sci.* **2015**, *351*, 920–926.
44. Xiao, J.; Chaudhuri, S. Design of anti-icing coatings using supercooled droplets as nano-to-microscale probes. *Langmuir* **2012**, *28*, 4434–4446.

45. Charpentier, T.V.; Neville, A.; Millner, P.; Hewson, R.; Morina, A. An investigation of freezing of supercooled water on anti-freeze protein modified surfaces. *J. Bionic Eng.* **2013**, *10*, 139–147.
46. Fu, Q.; Liu, E.; Wilson, P.; Chen, Z. Ice nucleation behaviour on sol–gel coatings with different surface energy and roughness. *Phys. Chem. Chem. Phys.* **2015**, *17*, 21492–21500.
47. Nosonovsky, M.; Hejazi, V. Why superhydrophobic surfaces are not always icephobic. *ACS Nano* **2012**, *6*, 8488–8491.
48. Lee, M.; Yim, C.; Jeon, S. Communication: Anti-icing characteristics of superhydrophobic surfaces investigated by quartz crystal microresonators. *J. Chem. Phys.* **2015**, *142*, 041102.
49. Subramanyam, S.B.; Rykaczewski, K.; Varanasi, K.K. Ice adhesion on lubricant-impregnated textured surfaces. *Langmuir* **2013**, *29*, 13414–13418.
50. Chanda, J.; Ionov, L.; Kirillova, A.; Synytska, A. New insight into icing and de-icing properties of hydrophobic and hydrophilic structured surfaces based on core–shell particles. *Soft Matter* **2015**, *11*, 9126–9134.
51. Guadarrama-Cetina, J.; Mongruel, A.; González-Viñas, W.; Beysens, D. Frost formation with salt. *EPL (Europhys. Lett.)* **2015**, *110*, 56002.
52. Carpenter, K.; Bahadur, V. Saltwater icephobicity: Influence of surface chemistry on saltwater icing. *Sci. Rep.* **2015**, *5*, doi:10.1038/srep17563.
53. Jiang, C.; Li, W. A facile method for preparations of micro-nanotextured Co₃O₄ films with the excellent superhydrophobic and anti-icing behavior. *Mater. Lett.* **2014**, *122*, 133–138.
54. Stone, H.A. Ice-phobic surfaces that are wet. *ACS Nano* **2012**, *6*, 6536–6540.
55. Gross, A.F.; Nowak, A.P.; Carter, W. Structural Coatings with Dewetting and Anti-Icing Properties, and Processes for Fabricating These Coatings. U.S. Pat. App. 13/836,208, 2013.
56. Momen, G.; Jafari, R.; Farzaneh, M. Ice repellency behaviour of superhydrophobic surfaces: Effects of atmospheric icing conditions and surface roughness. *Appl. Surf. Sci.* **2015**, *349*, 211–218.
57. Zhang, Q.; He, M.; Zeng, X.; Li, K.; Cui, D.; Chen, J.; Wang, J.; Song, Y.; Jiang, L. Condensation mode determines the freezing of condensed water on solid surfaces. *Soft Matter* **2012**, *8*, 8285–8288.
58. Wang, Y.; Yao, X.; Chen, J.; He, Z.; Liu, J.; Li, Q.; Wang, J.; Jiang, L. Organogel as durable anti-icing coatings. *Sci. China Mater.* **2015**, *58*, 559–565.
59. Jung, S.; Tiwari, M.K.; Doan, N.V.; Poulikakos, D. Mechanism of supercooled droplet freezing on surfaces. *Nat. Commun.* **2012**, *3*, 615.
60. Zhang, X.X.; Chen, M.; Fu, M. Impact of surface nanostructure on ice nucleation. *J. Chem. Phys.* **2014**, *141*, 124709.
61. Alizadeh, A.; Bahadur, V.; Kulkarni, A.; Yamada, M.; Ruud, J.A. Hydrophobic surfaces for control and enhancement of water phase transitions. *MRS Bull.* **2013**, *38*, 407–411.
62. Sun, X.; Damle, V.G.; Liu, S.; Rykaczewski, K. Bioinspired Stimuli-Responsive and Antifreeze-Secreting Anti-Icing Coatings. *Adv. Mater. Interfaces* **2015**, *2*, doi:10.1002/admi.201400479.
63. Tarquini, S.; Antonini, C.; Amirfazli, A.; Marengo, M.; Palacios, J. Investigation of ice shedding properties of superhydrophobic coatings on helicopter blades. *Cold Reg. Sci. Technol.* **2014**, *100*, 50–58.
64. He, Y.; Jiang, C.; Hu, P.; Yang, R.; Tian, W.; Yuan, W. Reducing ice accumulation and adhesion by using a flexible micro-rod film. *Cold Reg. Sci. Technol.* **2015**, *118*, 57–63.
65. Bahadur, V.; Mishchenko, L.; Hatton, B.; Taylor, J.A.; Aizenberg, J.; Krupenkin, T. Predictive model for ice formation on superhydrophobic surfaces. *Langmuir* **2011**, *27*, 14143–14150.
66. Zuo, Z.; Liao, R.; Guo, C.; Yuan, Y.; Zhao, X.; Zhuang, A.; Zhang, Y. Fabrication and anti-icing property of coral-like superhydrophobic aluminum surface. *Appl. Surf. Sci.* **2015**, *331*, 132–139.
67. Zhu, L.; Xue, J.; Wang, Y.; Chen, Q.; Ding, J.; Wang, Q. Ice-phobic coatings based on silicon-oil-infused polydimethylsiloxane. *ACS Appl. Mater. Interfaces* **2013**, *5*, 4053–4062.
68. Wang, Z.; Cong, Y.; Zhang, B. Liquid crystal compound anti-ice surface. *Liq. Cryst.* **2015**, *1–8*, doi:10.1080/02678292.2015.1100337.
69. Fitzner, M.; Sosso, G.C.; Cox, S.J.; Michaelides, A. The Many Faces of Heterogeneous Ice Nucleation: Interplay Between Surface Morphology and Hydrophobicity. *J. Am. Chem. Soc.* **2015**, *137*, 13658–13669.
70. Singh, J.K.; Müller-Plathe, F. On the characterization of crystallization and ice adhesion on smooth and rough surfaces using molecular dynamics. *Appl. Phys. Lett.* **2014**, *104*, 021603.

71. Alizadeh, A.; Bahadur, V.; Shang, W.; Zhu, Y.; Buckley, D.; Dhinojwala, A.; Sohal, M. Influence of substrate elasticity on droplet impact dynamics. *Langmuir* **2013**, *29*, 4520–4524.
72. He, Y.; Jiang, C.; Cao, X.; Chen, J.; Tian, W.; Yuan, W. Reducing ice adhesion by hierarchical micro-nano-pillars. *Appl. Surf. Sci.* **2014**, *305*, 589–595.
73. Hao, P.; Lv, C.; Zhang, X. Freezing of sessile water droplets on surfaces with various roughness and wettability. *Appl. Phys. Lett.* **2014**, *104*, 161609.
74. Arianpour, F.; Farzaneh, M. On Hydrophobic and Icephobic Properties of TiO₂-Doped Silicon Rubber Coatings. *J. ISSN* **2012**, *1*, 79–85.
75. Hu, J.; Xu, K.; Wu, Y.; Lan, B.; Jiang, X.; Shu, L. The freezing process of continuously sprayed water droplets on the superhydrophobic silicone acrylate resin coating surface. *Appl. Surf. Sci.* **2014**, *317*, 534–544.
76. Fillion, R.; Riahi, A.; Edrissy, A. A review of icing prevention in photovoltaic devices by surface engineering. *Renew. Sustain. Energy Rev.* **2014**, *32*, 797–809.
77. Kulinich, S.; Honda, M.; Zhu, A.; Rozhin, A.; Du, X. The icephobic performance of alkyl-grafted aluminum surfaces. *Soft Matter* **2015**, *11*, 856–861.
78. Rykaczewski, K.; Anand, S.; Subramanyam, S.B.; Varanasi, K.K. Mechanism of frost formation on lubricant-impregnated surfaces. *Langmuir* **2013**, *29*, 5230–5238.
79. Oberli, L.; Caruso, D.; Hall, C.; Fabretto, M.; Murphy, P.J.; Evans, D. Condensation and freezing of droplets on superhydrophobic surfaces. *Adv. Colloid Interface Sci.* **2014**, *210*, 47–57.
80. Xu, Q.; Li, J.; Tian, J.; Zhu, J.; Gao, X. Energy-Effective Frost-Free Coatings Based on Superhydrophobic Aligned Nanocones. *ACS Appl. Mater. Interfaces* **2014**, *6*, 8976–8980.
81. Liao, R.; Zuo, Z.; Guo, C.; Yuan, Y.; Zhuang, A. Fabrication of superhydrophobic surface on aluminum by continuous chemical etching and its anti-icing property. *Appl. Surf. Sci.* **2014**, *317*, 701–709.
82. Boreyko, J.B.; Collier, C.P. Delayed frost growth on jumping-drop superhydrophobic surfaces. *ACS Nano* **2013**, *7*, 1618–1627.
83. Chen, X.; Ma, R.; Zhou, H.; Zhou, X.; Che, L.; Yao, S.; Wang, Z. Activating the microscale edge effect in a hierarchical surface for frosting suppression and defrosting promotion. *Sci. Rep.* **2013**, *3*, doi:10.1038/srep02515.
84. Hao, Q.; Pang, Y.; Zhao, Y.; Zhang, J.; Feng, J.; Yao, S. Mechanism of Delayed Frost Growth on Superhydrophobic Surfaces with Jumping Condensates: More Than Interdrop Freezing. *Langmuir* **2014**, *30*, 15416–15422.
85. Lazauskas, A.; Guobienė, A.; Prosyčėvas, I.; Baltrušaitis, V.; Grigaliūnas, V.; Narmontas, P.; Baltrusaitis, J. Water droplet behavior on superhydrophobic SiO₂ nanocomposite films during icing/deicing cycles. *Mater. Charact.* **2013**, *82*, 9–16.
86. Sohn, Y.; Kim, D.; Lee, S.; Yin, M.; Song, J.Y.; Hwang, W.; Park, S.; Kim, H.; Ko, Y.; Han, I. Anti-frost coatings containing carbon nanotube composite with reliable thermal cyclic property. *J. Mater. Chem. A* **2014**, *2*, 11465–11471.
87. Haji-Akbari, A.; Debenedetti, P.G. Direct Calculation of Ice Homogeneous Nucleation Rate for a Molecular Model of Water. *Proc. Natl. Acad. Sci.* **2015**, *112*, 10582–10588.
88. Yeong, Y.H.; Mudafort, R.; Steele, A.; Bayer, I.; Loth, E. Water droplet impact dynamics at icing conditions with and without superhydrophobicity. In Proceedings of the 4th American Institute of Aeronautics & Astronautics, Atmospheric and Space Environments Conference, New Orleans, LA, USA, 25–28 June 2012; Volume 3134.
89. Hejazi, V.; Sobolev, K.; Nosonovsky, M. From superhydrophobicity to icephobicity: Forces and interaction analysis. *Sci. Rep.* **2013**, *3*, doi:10.1038/srep02194.
90. Han, S.W.; Jeong, J.; Lee, D.H. Ice-phobic behavior of superhydrophobic Al surface under various etching conditions. *J. Electroceramics* **2014**, *33*, 82–88.
91. Wu, Y.; Liu, Z.; Liang, Y.; Pei, X.; Zhou, F.; Xue, Q. Switching fluid slippage on pH-responsive superhydrophobic surfaces. *Langmuir* **2014**, *30*, 6463–6468.
92. Ramachandran, R.; Sobolev, K.; Nosonovsky, M. Dynamics of Droplet Impact on Hydrophobic/Icephobic Concrete with the Potential for Superhydrophobicity. *Langmuir* **2015**, *31*, 1437–1444.
93. Li, H.; Roisman, I.V.; Tropea, C. Influence of solidification on the impact of supercooled water drops onto cold surfaces. *Exp. Fluids* **2015**, *56*, 1–13.

94. Morgan, C.; Bossanyi, E.; Seifert, H. Assessment of safety risks arising from wind turbine icing. In Proceedings of the EWEC-Conference, Dublin, Germany, 6–9 October 1997; pp. 141–144.
95. Dalili, N.; Edrissy, A.; Carriveau, R. A review of surface engineering issues critical to wind turbine performance. *Renew. Sustain. Energy Rev.* **2009**, *13*, 428–438.
96. Sullivan, C.R.; Petrenko, V.F.; Mccurdy, J.D.; Kozliouk, V. Breaking the ice [transmission line icing]. *IEEE Ind. Appl. Mag.* **2003**, *9*, 49–54.
97. Petrenko, V.F. Systems and Methods for Modifying Ice Adhesion Strength. U.S. Patent 6,027,075, 2000.
98. Thomas, S.K.; Cassoni, R.P.; MacArthur, C.D. Aircraft anti-icing and de-icing techniques and modeling. *J. Aircr.* **1996**, *33*, 841–854.
99. Stolarczyk, L.G.; Stolarczyk, G.L. Ice Detection Apparatus for Transportation Safety. U.S. Patent 5,474,261, 1995.
100. Shotton, J.A. Mixtures of Acyclic Polyhydroxy Alcohols and Glycol Ethers as Anti-Icing Additives for Hydrocarbon Fuels. U.S. Patent 3,032,971, 1962.
101. Sapienza, R. Environmentally Benign Anti-Icing or Deicing Fluids. U.S. Patent 6,129,857, 2000.
102. Hommel, E.L.; Merle, J.K.; Ma, G.; Hadad, C.M.; Allen, H.C. Spectroscopic and computational studies of aqueous ethylene glycol solution surfaces. *J. Phys. Chem. B* **2005**, *109*, 811–818.
103. Smith, J.G., Jr.; Wohl, C.J.; Kreeger, R.E.; Hadley, K.R.; McDougall, N. *Hydrogen-Bonding Surfaces for Ice Mitigation*; National Aeronautics and Space Administration, Langley Research Center: Hampton, VA, USA, 2014.
104. Flemming, R.J.; Olsen, E.G. Passive Control of Ice Shedding. U.S. Patent 8,770,512, 2014.
105. Farhadi, S.; Farzaneh, M.; Kulinich, S. Anti-icing performance of superhydrophobic surfaces. *Appl. Surf. Sci.* **2011**, *257*, 6264–6269.
106. Antonini, C.; Innocenti, M.; Horn, T.; Marengo, M.; Amirfazli, A. Understanding the effect of superhydrophobic coatings on energy reduction in anti-icing systems. *Cold Reg. Sci. Technol.* **2011**, *67*, 58–67.
107. Passoni, L.; Bonvini, G.; Luzio, A.; Facibeni, A.; Bottani, C.E.; Di Fonzo, F. Multiscale effect of hierarchical self-assembled nanostructures on superhydrophobic surface. *Langmuir* **2014**, *30*, 13581–13587.
108. Lai, Y.K.; Chen, Z.; Lin, C.J. Recent progress on the superhydrophobic surfaces with special adhesion: From natural to biomimetic to functional. *J. Nanoeng. Nanomanuf.* **2011**, *1*, 18–34.
109. Maitra, T.; Tiwari, M.K.; Antonini, C.; Schoch, P.; Jung, S.; Eberle, P.; Poulikakos, D. On the nanoengineering of superhydrophobic and impalement resistant surface textures below the freezing temperature. *Nano Lett.* **2013**, *14*, 172–182.
110. Jung, S.; Dorrestijn, M.; Raps, D.; Das, A.; Megaridis, C.M.; Poulikakos, D. Are superhydrophobic surfaces best for icephobicity? *Langmuir* **2011**, *27*, 3059–3066.
111. Skarmoutsou, A.; Charitidis, C.; Gnanappa, A.; Tserepi, A.; Gogolides, E. Nanomechanical and nanotribological properties of plasma nanotextured superhydrophilic and superhydrophobic polymeric surfaces. *Nanotechnology* **2012**, *23*, 505711.
112. Gogolides, E.; Ellinas, K.; Tserepi, A. Hierarchical micro and nano structured, hydrophilic, superhydrophobic and superoleophobic surfaces incorporated in microfluidics, microarrays and lab on chip microsystems. *Microelectron. Eng.* **2015**, *132*, 135–155.
113. Dyett, B.P.; Wu, A.H.; Lamb, R.N. Mechanical Stability of Surface Architecture—Consequences for Superhydrophobicity. *ACS Appl. Mater. Interfaces* **2014**, *6*, 18380–18394.
114. Ellinas, K.; Pujari, S.P.; Dragatogiannis, D.A.; Charitidis, C.A.; Tserepi, A.; Zuilhof, H.; Gogolides, E. Plasma Micro-Nanotextured, Scratch, Water and Hexadecane Resistant, Superhydrophobic, and Superamphiphobic Polymeric Surfaces with Perfluorinated Monolayers. *ACS Appl. Mater. Interfaces* **2014**, *6*, 6510–6524.
115. Jafari, R.; Menini, R.; Farzaneh, M. Superhydrophobic and icephobic surfaces prepared by RF-sputtered polytetrafluoroethylene coatings. *Appl. Surf. Sci.* **2010**, *257*, 1540–1543.
116. Wang, N.; Xiong, D.; Li, M.; Deng, Y.; Shi, Y.; Wang, K. Superhydrophobic surface on steel substrate and its anti-icing property in condensing conditions. *Appl. Surf. Sci.* **2015**, *355*, 226–232.
117. Darmanin, T.; Guittard, F. Recent advances in the potential applications of bioinspired superhydrophobic materials. *J. Mater. Chem. A* **2014**, *2*, 16319–16359.
118. Gao, D.; Jones, A.K.; Sikka, V.K. Anti-Icing Superhydrophobic Coatings. U.S. Pat. App. 12/815,535, 2010.
119. Liu, K.; Jiang, L. Bio-inspired self-cleaning surfaces. *Annu. Rev. Mater. Res.* **2012**, *42*, 231–263.
120. Li, L.; Huang, T.; Lei, J.; He, J.; Qu, L.; Huang, P.; Zhou, W.; Li, N.; Pan, F. Robust Biomimetic-Structural Superhydrophobic Surface on Aluminum Alloy. *ACS Appl. Mater. Interfaces* **2015**, *7*, 1449–1457.

121. Victor, J.J.; Erb, U.; Palumbo, G. Micro/Nanoroughness Structures on Superhydrophobic Polymer Surfaces. In *The Nano-Micro Interface: Bridging the Micro and Nano Worlds*; Wiley-VCH: Weinheim, Germany, 2015; pp. 95–114.
122. Liu, Y.; Bai, Y.; Jin, J.; Tian, L.; Han, Z.; Ren, L. Facile fabrication of biomimetic superhydrophobic surface with anti-frosting on stainless steel substrate. *Appl. Surf. Sci.* **2015**, *355*, 1238–1244.
123. Liu, Y.; Liu, J.; Li, S.; Wang, Y.; Han, Z.; Ren, L. One-step method for fabrication of biomimetic superhydrophobic surface on aluminum alloy. *Colloids Surf. A Physicochem. Eng. Asp.* **2015**, *466*, 125–131.
124. Li, Y.; John, J.; Kolewe, K.W.; Schiffman, J.D.; Carter, K.R. Scaling up Nature: Large Area Flexible Biomimetic Surfaces. *ACS Appl. Mater. Interfaces* **2015**, *7*, 23439–23444.
125. Guo, Z.; Liu, W.; Su, B.L. Superhydrophobic surfaces: From natural to biomimetic to functional. *J. Colloid Interface Sci.* **2011**, *353*, 335–355.
126. Shen, Y.; Tao, H.; Chen, S.; Zhu, L.; Wang, T.; Tao, J. Icephobic/anti-icing potential of superhydrophobic Ti6Al4V surfaces with hierarchical textures. *RSC Adv.* **2015**, *5*, 1666–1672.
127. Liu, F.; Pan, Q. Facile Fabrication of Robust Ice-Phobic Polyurethane Sponges. *Adv. Mater. Interfaces* **2015**, *2*, doi:10.1002/admi.201500219.
128. Schutzius, T.M.; Jung, S.; Maitra, T.; Graeber, G.; Köhme, M.; Poulikakos, D. Spontaneous droplet trampolining on rigid superhydrophobic surfaces. *Nature* **2015**, *527*, 82–85.
129. Fletcher, N. Size effect in heterogeneous nucleation. *J. Chem. Phys.* **1958**, *29*, 572–576.
130. Schutzius, T.M.; Jung, S.; Maitra, T.; Eberle, P.; Antonini, C.; Stamatopoulos, C.; Poulikakos, D. Physics of Icing and Rational Design of Surfaces with Extraordinary Icephobicity. *Langmuir* **2014**, *31*, 4807–4821.
131. Eberle, P.; Tiwari, M.K.; Maitra, T.; Poulikakos, D. Rational nanostructuring of surfaces for extraordinary icephobicity. *Nanoscale* **2014**, *6*, 4874–4881.
132. Kulinich, S.; Farzaneh, M. On ice-releasing properties of rough hydrophobic coatings. *Cold Reg. Sci. Technol.* **2011**, *65*, 60–64.
133. Campbell, J.M.; Meldrum, F.C.; Christenson, H.K. Is ice nucleation from supercooled water insensitive to surface roughness? *J. Phys. Chem. C* **2015**, *119*, 1164–1169.
134. Petrenko, V.F. *Study of The Physical Mechanisms of Ice Adhesion*; Defense Technical Information Center: Fort Belvoir, VA, USA, 2003.
135. Zhang, J.; Kang, J.; Hu, P.; Meng, Q. Surface modification of poly (propylene carbonate) by oxygen ion implantation. *Appl. Surf. Sci.* **2007**, *253*, 5436–5441.
136. Zhu, H.; Jha, K.C.; Bhatta, R.S.; Tsige, M.; Dhinojwala, A. Molecular Structure of Poly (methyl methacrylate) Surface. I. Combination of Interface-Sensitive Infrared-Visible Sum Frequency Generation, Molecular Dynamics Simulations, and *ab Initio* Calculations. *Langmuir* **2014**, *30*, 11609–11618.
137. Jha, K.C.; Zhu, H.; Dhinojwala, A.; Tsige, M. Molecular Structure of Poly (methyl methacrylate) Surface II: Effect of Stereoregularity Examined through All-Atom Molecular Dynamics. *Langmuir* **2014**, *30*, 12775–12785.
138. Jha, K.C.; Dhinojwala, A.; Tsige, M. Local Structure Contributions to Surface Tension of a Stereoregular Polymer. *ACS Macro Lett.* **2015**, *4*, 1234–1238.
139. Yimer, Y.Y.; Jha, K.C.; Tsige, M. Epitaxial transfer through end-group coordination modulates the odd–even effect in an alkanethiol monolayer assembly. *Nanoscale* **2014**, *6*, 3496–3502.
140. Yeong, Y.; Loth, E.; Sokhey, J.; Lambourne, A. Ice Adhesion Strength on Hydrophobic and Superhydrophobic Coatings. In Proceedings of the 6th AIAA Atmospheric and Space Environments Conference, Atlanta, GA, USA, 16–20 June 2014; pp. 51–69.
141. Alizadeh, A.; Yamada, M.; Li, R.; Shang, W.; Otta, S.; Zhong, S.; Ge, L.; Dhinojwala, A.; Conway, K.R.; Bahadur, V.; *et al.* Dynamics of ice nucleation on water repellent surfaces. *Langmuir* **2012**, *28*, 3180–3186.
142. Boinovich, L.B.; Emelyanenko, A.M.; Ivanov, V.K.; Pashinin, A.S. Durable icephobic coating for stainless steel. *ACS Appl. Mater. Interfaces* **2013**, *5*, 2549–2554.
143. Chu, M.; Scavuzzo, R. Adhesive shear strength of impact ice. *AIAA J.* **1991**, *29*, 1921–1926.
144. Wang, D.; Tao, T.; Xu, G.; Luo, A.; Kang, S. Experimental study on frosting suppression for a finned-tube evaporator using ultrasonic vibration. *Exp. Therm. Fluid Sci.* **2012**, *36*, 1–11.
145. Brassard, J.; Sarkar, D.; Perron, J.; Audibert-Hayet, A.; Melot, D. Nano-micro structured superhydrophobic zinc coating on steel for prevention of corrosion and ice adhesion. *J. Colloid Interface Sci.* **2015**, *447*, 240–247.
146. Wang, C. Toward Polymer Coatings with Easy Ice Release. Ph.D. Thesis, Virginia Commonwealth University Richmond, Richmond, VA, USA, 2014.

147. Dai, X.; Stogin, B.B.; Yang, S.; Wong, T.S. Slippery Wenzel State. *ACS Nano* **2015**, *9*, 9260–9267.
148. He, M.; Song, Y.; Liu, B. Anti-Frost Coating and the Application Method Thereof. U.S. Patent 8,372,484, 2013.
149. Tourkine, P.; Le Merrer, M.; Quéré, D. Delayed freezing on water repellent materials. *Langmuir* **2009**, *25*, 7214–7216.
150. Mandal, D.K.; Criscione, A.; Tropea, C.; Amirfazli, A. Shedding of water drops from a surface under icing conditions. *Langmuir* **2015**, *31*, 9340–9347.
151. Mittal, K. *Advances in Contact Angle, Wettability and Adhesion, Volume Two*; John Wiley & Sons: Hoboken, NJ, USA, 2015.
152. Liu, Q.; Yang, Y.; Huang, M.; Zhou, Y.; Liu, Y.; Liang, X. Durability of a lubricant-infused Electro spray Silicon Rubber surface as an anti-icing coating. *Appl. Surf. Sci.* **2015**, *346*, 68–76.
153. Chernyy, S.; Järn, M.; Shimizu, K.; Swerin, A.; Pedersen, S.U.; Daasbjerg, K.; Makkonen, L.; Claesson, P.; Iruthayaraj, J. Superhydrophilic Polyelectrolyte Brush Layers with Imparted Anti-Icing Properties: Effect of Counter ions. *ACS Appl. Mater. Interfaces* **2014**, *6*, 6487–6496.
154. Azzaroni, O.; Brown, A.A.; Huck, W.T. Tunable wettability by clicking counterions into polyelectrolyte brushes. *Adv. Mater.* **2007**, *19*, 151–154.
155. Fletcher, N. Surface structure of water and ice. *Philos. Mag.* **1962**, *7*, 255–269.
156. Jellinek, H.H.G. Liquid-like (transition) layer on ice. *J. Colloid Interface Sci.* **1967**, *25*, 192–205.
157. Petrenko, V.F. Study of the surface of ice, ice/solid and ice/liquid interfaces with scanning force microscopy. *J. Phys. Chem. B* **1997**, *101*, 6276–6281.
158. Engemann, S.; Reichert, H.; Dosch, H.; Bilgram, J.; Honkimäki, V.; Snigirev, A. Interfacial melting of ice in contact with SiO₂. *Phys. Rev. Lett.* **2004**, *92*, 205701.
159. Marcus, Y. Effect of ions on the structure of water: Structure making and breaking. *Chem. Rev.* **2009**, *109*, 1346–1370.
160. Kasuya, M.; Hino, M.; Yamada, H.; Mizukami, M.; Mori, H.; Kajita, S.; Ohmori, T.; Suzuki, A.; Kurihara, K. Characterization of Water confined between Silica surfaces using the resonance shear measurement. *J. Phys. Chem. C* **2013**, *117*, 13540–13546.
161. Bekele, S.; Tsige, M. Interfacial Properties of Oxidized Polystyrene and Its Interaction with Water. *Langmuir* **2013**, *29*, 13230–13238.
162. Hirata, T.; Matsuno, H.; Kawaguchi, D.; Yamada, N.L.; Tanaka, M.; Tanaka, K. Effect of interfacial structure on bioinert property of poly (2-methoxyethyl acrylate)/poly (methyl methacrylate) blend films in water. *Phys. Chem. Chem. Phys.* **2015**, doi:10.1039/C5CP01972A.
163. Hirata, T.; Matsuno, H.; Kawaguchi, D.; Hirai, T.; Yamada, N.L.; Tanaka, M.; Tanaka, K. Effect of Local Chain Dynamics on a Bioinert Interface. *Langmuir* **2015**, *31*, 3661–3667.
164. Hirata, T.; Matsuno, H.; Kawaguchi, D.; Yamada, N.L.; Tanaka, M.; Tanaka, K. Construction of a blood-compatible interface based on surface segregation in a polymer blend. *Polymer* **2015**, *78*, 219–224.
165. Zhang, X.; Huang, Y.; Ma, Z.; Zhou, Y.; Sun, C.Q. *Mediation of Hydrogen-Bond Coupling Interactions by Programmable Heating and Salting*; Cornell University Library: Ithaca, NY, USA, 2013.
166. Congdon, T.; Notman, R.; Gibson, M.I. Antifreeze (glyco) protein mimetic behavior of poly (vinyl alcohol): detailed structure ice recrystallization inhibition activity study. *Biomacromolecules* **2013**, *14*, 1578–1586.
167. Zhou, J.; Anim-Danso, E.; Zhang, Y.; Zhou, Y.; Dhinojwala, A. Interfacial Water at Polyurethane-Sapphire Interface. *Langmuir* **2015**, *31*, 12401–12407.
168. Defante, A.P.; Burai, T.N.; Becker, M.L.; Dhinojwala, A. Consequences of Water between Two Hydrophobic Surfaces on Adhesion and Wetting. *Langmuir* **2015**, *31*, 2398–2406.
169. Loudon, P.B.; Gezelter, J.D. *The Different Facets of Ice Have Different Hydrophilicities: Friction at Water/Ice-Ih Interfaces*; Cornell University Library: Ithaca, NY, USA, 2015.
170. Khan, S.; Azimi, G.; Yildiz, B.; Varanasi, K.K. Role of surface oxygen-to-metal ratio on the wettability of rare-earth oxides. *Appl. Phys. Lett.* **2015**, *106*, 061601.
171. Zhang, X.; He, J. Hydrogen-Bonding-Supported Self-Healing Antifogging Thin Films. *Sci. Rep.* **2015**, *5*, doi:10.1038/srep09227.
172. Hofmeister, F. Zur lehre von der wirkung der salze. *Arch. Exp. Pathol. Pharmacol.* **1888**, *25*, 1–30.
173. Flores, S.C.; Kherb, J.; Konelick, N.; Chen, X.; Cremer, P.S. The effects of Hofmeister cations at negatively charged hydrophilic surfaces. *J. Phys. Chem. C* **2012**, *116*, 5730–5734.

174. Zhang, Y.; Cremer, P.S. Interactions between macromolecules and ions: The Hofmeister series. *Curr. Opin. Chem. Biol.* **2006**, *10*, 658–663.
175. Wang, Y.; Wohlerl, J.; BergenstraÛhle-Wohlerl, M.; Kochumalayil, J.J.; Berglund, L.A.; Tu, Y.; Ågren, H. Molecular Adhesion at Clay Nanocomposite Interfaces Depends on Counterion Hydration–Molecular Dynamics Simulation of Montmorillonite/Xyloglucan. *Biomacromolecules* **2014**, *16*, 257–265.
176. Heinz, H.; Jha, K.C.; Luettmmer-Strathmann, J.; Farmer, B.L.; Naik, R.R. Polarization at metal–Biomolecular interfaces in solution. *J. R. Soc. Interface* **2010**, *8*, 220–232.
177. Patwardhan, S.V.; Emami, F.S.; Berry, R.J.; Jones, S.E.; Naik, R.R.; Deschaume, O.; Heinz, H.; Perry, C.C. Chemistry of aqueous silica nanoparticle surfaces and the mechanism of selective peptide adsorption. *J. Am. Chem. Soc.* **2012**, *134*, 6244–6256.
178. Amarpuri, G.; Zhang, C.; Diaz, C.; Opell, B.D.; Blackledge, T.A.; Dhinojwala, A. Spiders Tune Glue Viscosity to Maximize Adhesion. *ACS Nano* **2015**, *9*, 11472–11478.
179. Amarpuri, G.; Chaurasia, V.; Jain, D.; Blackledge, T.A.; Dhinojwala, A. Ubiquitous distribution of salts and proteins in spider glue enhances spider silk adhesion. *Sci. Rep.* **2015**, *5*, doi:10.1038/srep09030.
180. Oncsik, T.; Trefalt, G.; Borkovec, M.; Szilagy, I. Specific ion effects on particle aggregation induced by monovalent salts within the Hofmeister series. *Langmuir* **2015**, *31*, 3799–3807.
181. Barrie, L. Snow formation and processes in the atmosphere that influence its chemical composition. In *Seasonal Snowpacks*; Springer: Berlin, Germany; Heidelberg, Germany, 1991; pp. 1–20.
182. Sihvonen, S.K.; Schill, G.P.; Lykтей, N.A.; Veghte, D.P.; Tolbert, M.A.; Freedman, M.A. Chemical and Physical Transformations of Aluminosilicate Clay Minerals Due to Acid Treatment and Consequences for Heterogeneous Ice Nucleation. *J. Phys. Chem. A* **2014**, *118*, 8787–8796.
183. Stack, A.G. Precipitation in pores: A geochemical frontier. *Rev. Miner. Geochem.* **2015**, *80*, 165–190.
184. Anim-Danso, E.; Zhang, Y.; Alizadeh, A.; Dhinojwala, A. Freezing of water next to solid surfaces probed by infrared–visible sum frequency generation spectroscopy. *J. Am. Chem. Soc.* **2013**, *135*, 2734–2740.
185. Anim-Danso, E.; Zhang, Y.; Dhinojwala, A. Freezing and Melting of Salt Hydrates Next to Solid Surfaces Probed by Infrared–Visible Sum Frequency Generation Spectroscopy. *J. Am. Chem. Soc.* **2013**, *135*, 8496–8499.
186. Makkonen, L. Ice adhesion–theory, measurements and countermeasures. *J. Adhes. Sci. Technol.* **2012**, *26*, 413–445.
187. Zhang, Y.; Anim-Danso, E.; Dhinojwala, A. The Effect of a Solid Surface on the Segregation and Melting of Salt Hydrates. *J. Am. Chem. Soc.* **2014**, *136*, 14811–14820.
188. Fortin, G.; Perron, J. Ice adhesion models to predict shear stress at shedding. *J. Adhes. Sci. Technol.* **2012**, *26*, 523–553.
189. Ishiyama, T.; Takahashi, H.; Morita, A. Origin of vibrational spectroscopic response at ice surface. *J. Phys. Chem. Lett.* **2012**, *3*, 3001–3006.
190. Li Barnett, I.; Groenzin, H.; Shultz, M.J. Hydrogen bonding in the hexagonal ice surface. *J. Phys. Chem. A* **2010**, *115*, 6039–6045.
191. Zaera, F. Probing liquid/solid interfaces at the molecular level. *Chem. Rev.* **2012**, *112*, 2920–2986.
192. Friedman, S.R.; Khalil, M.; Taborek, P. Wetting transition in water. *Phys. Rev. Lett.* **2013**, *111*, 226101.
193. Cygan, R.T.; Liang, J.J.; Kalinichev, A.G. Molecular models of hydroxide, oxyhydroxide, and clay phases and the development of a general force field. *J. Phys. Chem. B* **2004**, *108*, 1255–1266.
194. Mark, P.; Nilsson, L. Structure and dynamics of the TIP3P, SPC, and SPC/E water models at 298 K. *J. Phys. Chem. A* **2001**, *105*, 9954–9960.
195. Taylor, R.S.; Dang, L.X.; Garrett, B.C. Molecular dynamics simulations of the liquid/vapor interface of SPC/E water. *J. Phys. Chem.* **1996**, *100*, 11720–11725.

